Four-probe measurements of the in-plane thermoelectric properties of nanofilms

Anastassios Mavrokefalos, Michael T. Pettes, Feng Zhou, and Li Shi[a)]
Department of Mechanical Engineering, The University of Texas at Austin, Austin, Texas 78712 and Center for Nano and Molecular Science and Technology, Texas Materials Institute, The University of Texas at Austin, Austin, Texas 78712

(Received 22 December 2006; accepted 30 January 2007; published online 14 March 2007)

Measuring in-plane thermoelectric properties of submicron thin films has remained a challenging task. Here we report a method based on a suspended microdevice for four-probe measurements of the Seebeck coefficient, thermal conductivity, electrical conductivity, and thermoelectric figure of merit of patterned indium arsenide (InAs) nanofilms assembled on the microdevice. The contact thermal resistance and intrinsic thermal resistance of the 40 nm thick InAs nanofilm sample were measured by using the nanofilm itself as a differential thermocouple to determine the temperature drops at the contacts. The microdevice was also used to measure a 190 nm thick silicon dioxide (SiO_2) film and the results were compared with those reported in the literature. A through-substrate hole under the suspended microdevice allows for transmission electron microscopy characterization of the nanofilm sample assembled on the device. This capability enables one to correlate the measured thermoelectric properties with the crystal structures of the nanofilm. © *2007 American Institute of Physics.* [DOI: 10.1063/1.2712894]

I. INTRODUCTION

Thin film thermoelectric materials are under active investigations for improving the energy efficiency of Peltier refrigerators and thermoelectric power generators. The energy efficiency of thermoelectric devices is limited by the thermoelectric figure of merit (ZT) defined as $ZT \equiv S^2 \sigma T / \kappa$ where S is the Seebeck coefficient, σ is the electrical conductivity, κ is the thermal conductivity, and T is the absolute temperature. The ZT of conventional bulk materials have remained at a value close to 1 or lower for the last 50 years. Recent reports of high ZT values in thin film superlattices[1] have stimulated intense interests in nanostructured materials with interfaces or embedded nanoparticles, which scatter phonons and reduce the lattice thermal conductivity.[2] Additionally, it was also suggested that electron energy quantization in thin film quantum well structures can increase the ZT via an increase in the power factor $S^2\sigma$.[3]

One of the major challenges in the research of thin film thermoelectric materials is to characterize the thermoelectric properties of thin films and relate them to their crystal structures. These thin films are often highly anisotropic with very different properties along the cross-plane and in-plane directions. While the 3ω method[4] and the time-domain laser reflectance technique[5] have been employed with success to measure the cross-plane thermal conductivity of thin films, measuring the in-plane thermal conductivity of thin films has been difficult because of parasitic heat conduction in the substrate. Ju *et al.* extended the 3ω method to obtain the in-plane thermal conductivity of a thin film by using microfabricated heater bridges of varying widths.[6] The thermal conductivity of the film was extracted by fitting a two-dimensional heat conduction model to the measurement results. To directly measure the in-plane thermal conductivity of a silicon thin film, Liu and Asheghi[7] patterned the film into a suspended beam and employed a metal layer on top of the patterned film as a heater and resistance thermometer. The uncertainty of the metal layer thickness and thermal conductivity introduces uncertainties to the measured thermal conductivity of the silicon film.

Technical issues also exist in measuring the in-plane electrical conductivity and Seebeck coefficient of thin films at high temperature, where the contribution from thermally generated carriers in a semi-insulating substrate cannot be ignored. Moreover, it is difficult to accurately measure the cross-plane electrical conductivity and Seebeck coefficient of thin films because of the influence of contact resistance and substrate resistance.

Here we report a new method for measuring the in-plane thermoelectric properties of thin film structures with thickness as thin as tens of nanometers. This method is a further development of a suspended microdevice[8,9] reported previously for measuring the thermal and thermoelectric properties of individual nanowire structures. The new measurement device reported here allows for four-probe measurements of the Seebeck coefficient, thermal conductivity, and electrical conductivity, so that the errors due to contact thermal and electrical resistances can be eliminated. Moreover, it allows for transmission electron microscopy (TEM) characterization of the patterned nanofilm structure assembled on the device, allowing one to establish the structure-thermoelectric property relationship of the nanofilm. This method has been employed to characterize 40 nm thick InAs films.

[a)]Author to whom correspondence should be addressed; electronic mail: lishi@mail.utexas.edu

 © 2007 American Institute of Physics

Downloaded 16 Mar 2007 to 146.6.84.239. Redistribution subject to AIP license or copyright, see http://rsi.aip.org/rsi/copyright.jsp

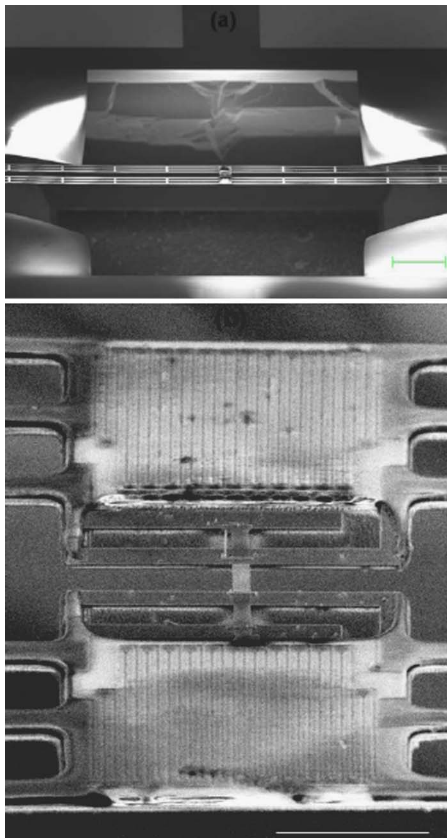

FIG. 1. Tilted SEMs of (a) the measurement device and (b) its two suspended membranes with an etched InAs nanofilm assembled in between. The scale bars are 100 and 10 μm in (a) and (b), respectively.

II. MEASUREMENT DEVICE AND SAMPLE PREPARATION

Figure 1 shows the scanning electron microscopy (SEM) images of the suspended microdevice with an InAs nanofim assembled on the device. The device consisted of two adjacent 20×20 μm^2 low-stress silicon nitride (SiN_x) membranes each suspended with six 420 μm long and 2 μm wide SiN_x beams. One platinum resistance thermometer (PRT) serpentine was patterned on each membrane, and connected to four Pt electrodes for measuring its four-probe electrical resistance. Two additional Pt electrodes were patterned on each membrane. Below the two membranes was a through-substrate hole. The device fabrication process is similar to that reported in an earlier work,[8] except that in the current work the Pt serpentine was patterned using electron beam lithography (EBL) and a back side masking step was added for etching the thorough-wafer hole using 5% tetramethylammonium hydroxide (TMAH) in water.

The InAs nanofilm was obtained by nanopatterning of a thin InAs film, as illustrated in Fig. 2. For the current study a 40 nm thick n-type InAs film was grown on a GaAs substrate using molecular beam epitaxy (MBE) with a targeted Si doping concentration of 3×10^{17} cm^{-3}. EBL was used to pattern arrays of ZEP520A resist lines with different widths ranging from 50 to 2000 nm. The resist line pattern was used as an etching mask during reactive ion etching (RIE) of the exposed InAs film with CH_4+H_2+Ar chemistry. After the pattern was transferred into the InAs film, the resist layer

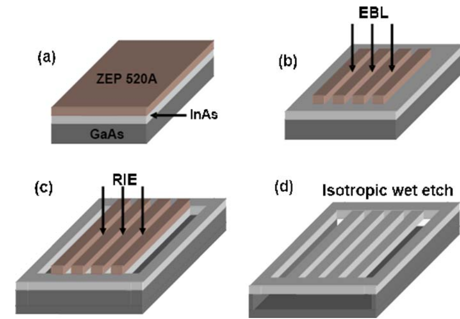

FIG. 2. (Color online) Fabrication process to pattern suspended InAs nanofilms from an epitaxial InAs film.

was stripped using oxygen plasma etching. Subsequently, the obtained InAs nanofilms of different widths were suspended by wet etching of the underlining GaAs substrate in a solution of 0.8M $K_3[Fe(CN)6]$ in 0.3M KOH:H_2O:glycerine (1:5:2), which had an isotropic etching rate for GaAs of about 40 nm/min.

The etched InAs nanofilm was transferred to the microdevice from the substrate with the help of a Zyvex S100 Nanomanipulator System installed in a SEM. A sharp tungsten tip of the nanomanipulator was actuated by nanometer resolution piezoelectric motors to cut the two ends of a suspended nanofilm and transport the nanofilm onto the microdevice.

Even though the nanofilm was placed on top of the four Pt electrodes on the microdevice, the native oxide on the surface of the nanofilm prevented electrical contact between the nanofilm and electrode. To improve electrical contact we used electron beam induced metal deposition (EBIMD) to deposit a 250 nm wide, 150 nm thick, 2 μm long Pt line pattern on top of the nanofilm and each underlying Pt electrode. Four such Pt line patterns on the nanofilm can be seen in Fig. 3. The 30 keV electron beam used in the EBIMD process could damage the native oxide and allowed for electrical contact between the deposited Pt and the nanofilm. To prevent Pt spreading, care was taken to limit the volume of the deposited Pt.

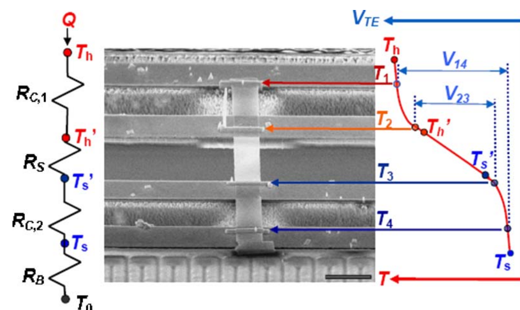

FIG. 3. (Color online) A schematic diagram of the thermal measurement methods. T_h and T_s are the temperatures of the heating (upper) and sensing (lower) membranes, respectively. T_1, T_2, T_3, and T_4 are the temperatures at the four Pt contacts deposited on the nanofilm. T_0 is the temperature of the substrate. R_S and R_B are the thermal resistances of the nanofilm and the six beams supporting one membrane, respectively. $R_{C,1}$ and $R_{C,2}$ are the contact thermal resistances between the nanofilm and the heating and sensing membranes, respectively. V_{14} and V_{23} are the thermoelectric voltage (V_{TE}) measured between the two outer electrodes and that between the two inner electrodes, respectively. The scale bar in the SEM image is 2 μm.

Downloaded 16 Mar 2007 to 146.6.84.239. Redistribution subject to AIP license or copyright, see http://rsi.aip.org/rsi/copyright.jsp

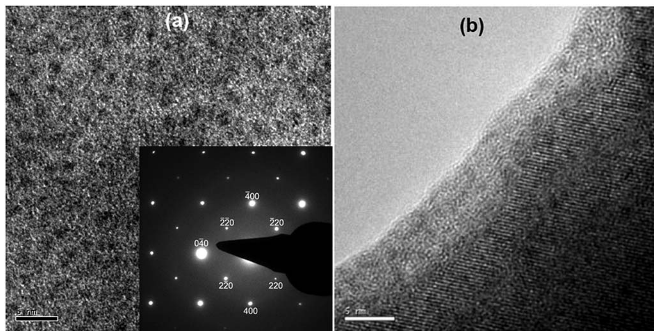

FIG. 4. (a) TEM of the suspended InAs nanofilm in Fig. 3 that was passivated with a $(NH_4)_2S$ solution. The inset is the selective area diffraction pattern. The scale bar is 5 nm. (b) TEM of another suspended InAs nanofilm sample that was not passivated with the $(NH_4)_2S$ solution. The scale bar is 5 nm.

The through-substrate hole under the two membranes allowed us to conduct TEM measurement of the InAs nanofilm assembled on the suspended device. Figure 4(a) shows the TEM image of the InAs nanofilm in Fig. 3 after Pt deposition on the four electrodes. This TEM image reveals an amorphous structure with black spots, and is distinctly different from the TEM image in Fig. 4(b) for another suspended InAs nanofilm that was patterned from the same parent InAs film and assembled on another device with Pt deposited on the four contacts. The TEM image in Fig. 4(b) reveals crystalline structure although the lattice fringes are not continuous and are broken by domains of apparently amorphous material. The lattice fringes tend to shift by a half period when they cross these domains. This may be due to some defects, dislocations, or grain boundaries that were caused by the large lattice mismatch of 6.686% between the InAs film and the GaAs substrate. The discontinuity is also likely due to the fact that the specimen thickness could be changing. A change in specimen thickness frequently necessitates a shift from bright to dark lattice fringe. Although the two different InAs nanofilm samples were patterned from the same parent InAs film, the amorphouslike sample in Fig. 4(a) was treated with an additional surface passivation procedure in a $(NH_4)_2S$ solution. This passivation step was not applied to the crystalline sample in Fig. 4(b) because the four deposited Pt lines made good electrical contact to the nanofilm without passivation of the nanofilm. We suspect that the passivation step was not carried out properly so that a thick amorphous layer formed on the surface of the passivated InAs nanofilm. The thick amorphous layer might have prevented TEM observation of the lattice fringe. In addition, the passivation process could have left islands of heavier In atoms on the surface that appeared as dark spots in Fig. 4(a). Despite this problem, the diffraction pattern obtained on this amorphous-like sample was found to be similar to that for crystalline InAs. The capability of TEM characterization of the nanofilm assembled on the measurement device provides valuable information for us to correlate the measured thermoelectric properties discussed in the following with the crystalline structure obtained by TEM on the same sample.

III. MEASUREMENT METHODS AND RESULTS

The thermoelectric measurements were conducted in a Janis ST-100 continuous flow liquid helium cryostat where the sample space is in high vacuum and the temperature range is 4–475 K. The thermal resistance of the nanofilm sample was obtained based partly on the procedure developed previously for nanowire samples.[8–10] When a direct current (I) was supplied to one PRT to raise the temperature (T_h) of one membrane, part of the Joule heat generated in this heating membrane, Q, was conducted through the nanofilm to the other membrane referred as the sensing membrane, increasing its temperature (T_s), as illustrated in Fig. 3. Because the internal thermal resistance of each membrane was on the order of 10^5 K/W and was two orders of magnitude smaller than the thermal resistance of the six beams supporting each membrane, the temperature distribution on each membrane was uniform during the heating process. The temperature uniformity has been verified in a finite element calculation.[11] The two PRTs were used to measure the temperature rises on the heating and sensing membranes at different I values, $\Delta T_h(I) \equiv T_h(I) - T_0$ and $\Delta T_s(I) \equiv T_s(I) - T_0$, respectively, where T_0 is the substrate temperature. The thermal resistance of the six beams supporting each membrane was obtained as

$$R_B = \frac{\Delta T_h + \Delta T_s}{Q_h + Q_L}, \tag{1}$$

where Q_h is the Joule heat dissipation in the PRT on the heating membrane, and Q_L is the Joule heat dissipation in one of the two identical Pt leads supplying the current to the heating PRT. According to the thermal circuit in Fig. 3,

$$R_{\text{total}} \equiv R_{C,1} + R_S + R_{C,2} = \frac{\Delta T_h - \Delta T_s}{Q}, \tag{2}$$

where R_S is thermal resistance of the suspended segment of the nanofilm sample, $R_{C,1}$ and $R_{C,2}$ are the contact thermal resistances between the nanofilm and the two membranes, and Q equals the heat conducted through the six beams of the sensing membrane to the substrate, which was obtained as

$$Q = R_B \Delta T_s. \tag{3}$$

The new design of the microdevice allowed us to investigate the contact thermal resistances ($R_{C,1}$ and $R_{C,2}$) between the suspended nanofilm and the two membranes. According to the temperature profile schematic shown in Fig. 3, the contact thermal resistances can cause temperature drops, i.e., $(T_h - T_h')$ and $(T_s' - T_s)$, where T_h' and T_s' are the temperatures at the two ends of the suspended segment of the nanofilm. While the temperature profile is linear along the suspended segment, the temperature decays approximately exponentially along the two segments in contact with the membranes, as illustrated in Fig. 3. In the experiment, we used the four Pt contacts deposited on the nanofilm to measure the following two thermoelectric voltages generated by the nanofilm due to the temperature differences,

$$V_{14} = S(T_1 - T_4) \tag{4a}$$

and

Downloaded 16 Mar 2007 to 146.6.84.239. Redistribution subject to AIP license or copyright, see http://rsi.aip.org/rsi/copyright.jsp

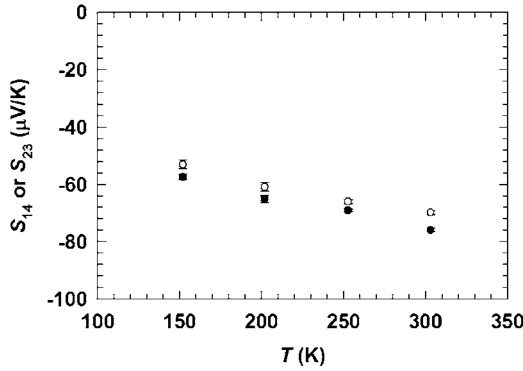

FIG. 5. Measured S_{14} (unfilled circles) and S_{23} (filled circles) as a function of temperature.

$$V_{23} = S(T_2 - T_3), \tag{4b}$$

where V_{14} and V_{23} are the thermoelectric voltage measured between the two outer electrodes and that between the two inner electrodes, respectively; S is the Seebeck coefficient of the nanofilm and is assumed to be uniform along the nanofilm and much larger than that of the Pt electrodes; and T_1, T_2, T_3 and T_4 are the temperatures at the four Pt contacts deposited on the nanofilm, as shown in Fig. 3.

We define

$$S_{14} \equiv \frac{V_{14}}{T_h - T_s} \tag{5a}$$

and

$$S_{23} \equiv \frac{V_{23}}{T_h - T_s}. \tag{5b}$$

The measurement results of S_{14} and S_{14} of the InAs nanofilm sample are shown in Fig. 5 as a function of temperature. As discussed in the following, the total contact resistance $R_C \equiv R_{C1} + R_{C2}$ and the sample thermal resistance R_S can be obtained from the ratio (γ) between S_{14} and S_{23}, i.e.,

$$\gamma \equiv \frac{S_{14}}{S_{23}} = \frac{T_1 - T_4}{T_2 - T_3}. \tag{6}$$

Figure 6 illustrates heat transfer between the two membranes through the suspended nanofilm and various length segments used in the following analysis. Because the temperature of each nanofilm segment in contact with one membrane varies along the length as a result of heat transfer between the nanofilm and the membrane, each nanofilm segment in contact with the membrane should be treated as a fin. The thermal contact resistance between the nanofilm and each membrane is thus the fin resistances, which can be calculated using the fin resistance formula[12]

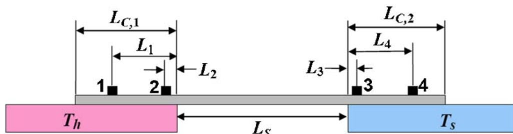

FIG. 6. (Color online) Schematic diagram of the nanofilm suspended between two suspended membranes indicating various length segments for the fin analysis.

$$R_{C,i} = \frac{1}{\kappa A m \tanh(m L_{C,i})}, \quad i = 1 \text{ or } 2, \tag{7}$$

where κ and A are the thermal conductivity and cross section area of the nanofilm, respectively, $L_{C,i}$ is the length of a nanofilm segment in contact with one membrane, and m is defined as

$$m = \sqrt{\frac{hw}{\kappa A}}, \tag{8}$$

where h is the thermal contact conductance per unit area between the nanofilm and the membrane, and w is the width of the nanofilm.

The thermal resistance of the suspended segment of the nanofilm is

$$R_S = \frac{L_S}{\kappa A}, \tag{9}$$

where L_S is the length of the suspended segment. According to the thermal resistance circuit in Fig. 3,

$$Q = \frac{T_h - T_h'}{R_{C,1}} = \frac{T_h' - T_s'}{R_S} = \frac{T_s' - T_s}{R_{C,2}}. \tag{10}$$

According to the fin temperature profile[12]

$$\frac{T_h - T_i}{T_h - T_h'} = \frac{\cosh[m(L_{C,1} - L_i)]}{\cosh(m L_{C,1})}, \quad i = 1 \text{ or } 2 \tag{11a}$$

and

$$\frac{T_i - T_s}{T_s' - T_s} = \frac{\cosh[m(L_{C,2} - L_i)]}{\cosh(m L_{C,2})}, \quad i = 3 \text{ or } 4. \tag{11b}$$

From Eqs. (9)–(11), we obtain

$$\gamma_{14} \equiv \frac{T_1 - T_4}{T_h' - T_s'} = 1 + \frac{1 - \cosh[m(L_{C,1} - L_1)]/\cosh(m L_{C,1})}{L_S m \tanh(m L_{C,1})} + \frac{1 - \cosh[m(L_{C,2} - L_4)]/\cosh(m L_{C,2})}{L_S m \tanh(m L_{C,2})}, \tag{12a}$$

$$\gamma_{23} \equiv \frac{T_2 - T_3}{T_h' - T_s'} = 1 + \frac{1 - \cosh[m(L_{C,1} - L_2)]/\cosh(m L_{C,1})}{L_S m \tanh(m L_{C,1})} + \frac{1 - \cosh[m(L_{C,2} - L_3)]/\cosh(m L_{C,2})}{L_S m \tanh(m L_{C,2})}, \tag{12b}$$

and

$$\gamma = \frac{T_1 - T_4}{T_2 - T_3} = \frac{\gamma_{14}}{\gamma_{23}}. \tag{12c}$$

The parameter m can be obtained based on Eq. (12) using the measured γ value at each temperature. The obtained m value is used to calculate γ_{23} according to Eq. (12b). We can derive the following equation to calculate the ratio α defined as

$$\alpha \equiv \frac{T_h - T_s}{T_h' - T_s'} = 1 + \frac{1}{L_S m}\left[\frac{1}{\tanh(m L_{C,1})} + \frac{1}{\tanh(m L_{C,2})}\right]. \tag{13}$$

Downloaded 16 Mar 2007 to 146.6.84.239. Redistribution subject to AIP license or copyright, see http://rsi.aip.org/rsi/copyright.jsp

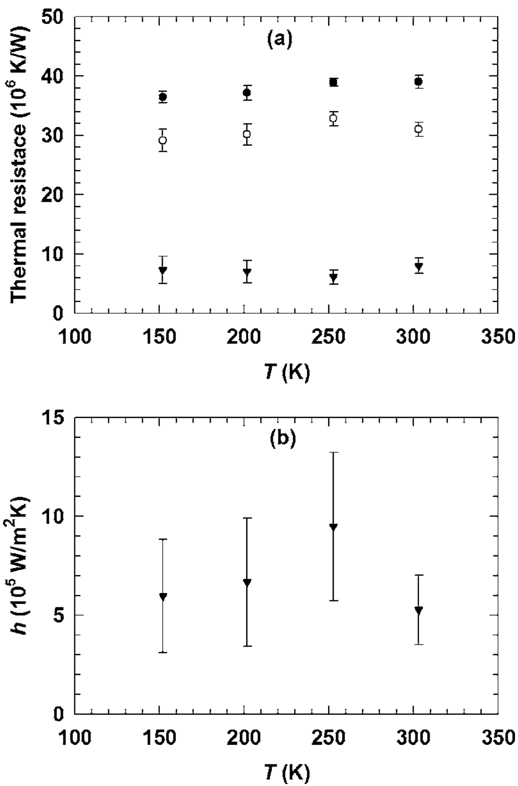

FIG. 7. (a) Measured R_{total} (filled circles), R_S (unfilled circles), and R_C (filled triangles) as a function of temperature for the InAs nanofilm. (b) Measured h as a function of temperature.

Using the α and γ_{23} values calculated based on the measured S_{14} and S_{23} results at each temperature, we obtain the Seebeck coefficient, the sample thermal resistance, and the contact thermal resistance as

$$S = \alpha S_{23}/\gamma_{23}, \tag{14a}$$

$$R_S = R_{\text{total}}/\alpha, \tag{14b}$$

and

$$R_C \equiv R_{\text{total}} - R_S. \tag{14c}$$

Figure 7(a) shows the obtained R_{total}, R_S, and R_C of the sample shown in Fig. 4(a). As shown in Fig. 7(b), the obtained h is comparable to the contact thermal conductance between aluminum and aluminum with metallic (Pb) coating.[12] Figure 8 shows the obtained Seebeck coefficient, the thermal conductivity from Eq. (9), the electrical conductivity from the measured four-probe electrical resistance, and $ZT = S^2\sigma T/k$ of the amorphouslike sample in Fig. 4(a). The electrical conductivity was obtained in a four-probe measurement setup, where the current flows between the two outer electrodes and the voltage drop between the two inner electrodes is measured with an electrometer of input impedance larger than $2 \times 10^{14}\ \Omega$.

The obtained Seebeck coefficient is negative, indicating that the film is n type, in agreement with the intended doping type during MBE growth. The electrical conductivity shows linear temperature dependence, suggesting nondegenerate doping. The thermal conductivity at room temperature is approximately 15 times smaller than the corresponding bulk values because of reduced phonon mean free path by the amorphous surface layer and also possibly due to grain boundary scattering of phonons in the remaining crystalline core of the nanofilm sample.

To verify that the Pt deposition process did not cause spreading, we have also conducted an experiment on a 190 ± 10 nm thick SiO_2 film thermally grown on a silicon substrate. The SiO_2 film was patterned based on the same EBL and RIE procedure and was suspended from the silicon substrate by a 15 min wet etching of the substrate in 5% TMAH in aqueous solution. The SiO_2 film was then as-

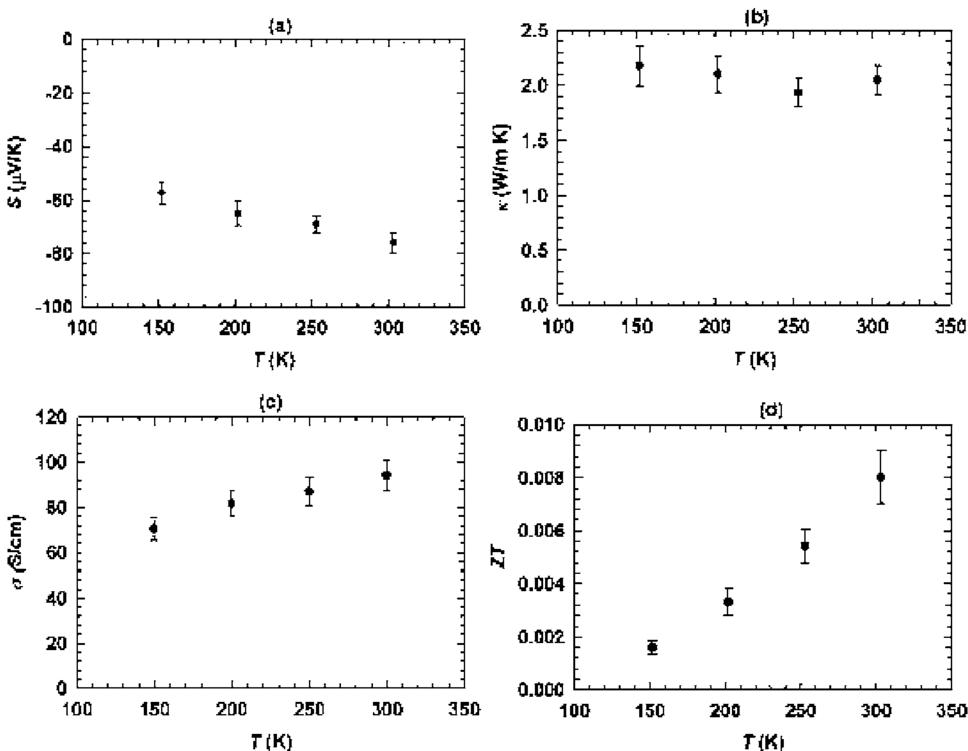

FIG. 8. Measured Seebeck coefficient S (a), thermal conductivity κ (b), electrical conductivity σ (c), and ZT (d) of the etched InAs nanofilm as a function of temperature. The figure of merit was calculated according to $ZT = S^2\sigma T/\kappa$.

Downloaded 16 Mar 2007 to 146.6.84.239. Redistribution subject to AIP license or copyright, see http://rsi.aip.org/rsi/copyright.jsp

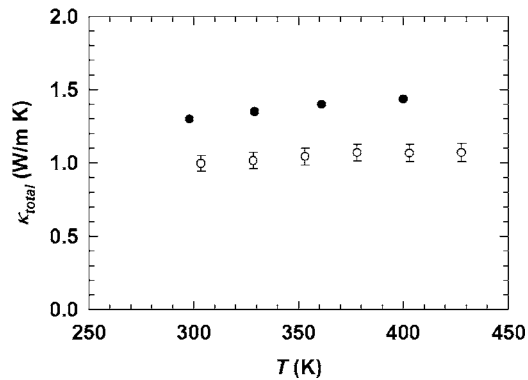

FIG. 9. κ_{total} of the 190±10 nm thick SiO_2 film (unfilled circles) as a function of temperature. The thermal conductivity data reported in Ref. 13 for a 0.99 μm thick SiO_2 film are shown as filled circles for comparison. Both films were thermally grown on a silicon substrate.

sembled on the microdevice using the nanomanipulator as described previously. Four narrow Pt lines were deposited on patterned SiO_2 film at the four Pt contacts. The Pt line dimension and separation were kept to be similar to those deposited on the InAs nanofilm. Two-probe electrical resistance measurements between any two of the four Pt contacts to the SiO_2 film yielded resistances larger than 10^{10} Ω, compared to 10^6 Ω measured for the InAs nanofilm. This test verifies that the Pt deposition method did not present noticeable spreading or contamination to the suspended film and the measured resistance and Seebeck coefficient of the InAs nanofilm were due to the nanofilm instead of a thin conducting metal organic compound coating on the nanofilm surface.

Because the nonconducting SiO_2 film could not be used as a thermocouple element for the measurement of the thermoelectric voltages V_{14} and V_{23}, the contact thermal resistance to the SiO_2 film could not be obtained using the aforementioned procedure. Instead, we have measured R_{total} of the SiO_2 film according to Eqs. (1)–(3) and calculated $\kappa_{\text{total}} = L_S/R_{\text{total}}A$. As shown in Fig. 9, the as-obtained κ_{total} of the SiO_2 film exhibits a similar trend as the thermal conductivity of a 0.99 μm thick SiO_2 film obtained by the 3ω method,[13] but at about 30% lower values. The lower values are attributed mainly to R_C that was not eliminated in the calculation of κ_{total}. For the InAs film, R_C was found to be about 15%–20% of R_{total}. The R_C/R_{total} ratio is expected to be higher for the thicker SiO_2 film than for the thinner InAs film because R_S decreases and R_C does not change much when the film thickness is increased. Consequently, for the SiO_2 film in the current work R_C could contribute to about 30% of R_{total} so that κ_{total} could be about 30% lower than κ. It is also possible that the thinner SiO_2 film in the current work has more voids and lower κ than the thicker film in Ref. 13. On the other hand, because the SiO_2 films are amorphous, we expect that the different thickness values should not yield much different κ for the two SiO_2 films. In addition, both of the SiO_2 films were amorphous so that κ should be rather isotropic with similar values along the in-plane direction measured in the current work and the cross-plane direction measured in Ref. 13.

IV. SUMMARY

We show that the new four-probe measurement procedure based on the microdevice can be used to obtain the in-plane Seebeck coefficient, thermal conductivity, electrical conductivity, and ZT of patterned thin films of tens of nanometer thickness. The contact thermal resistance and the intrinsic thermal resistance of the nanofilm sample can be obtained by using the nanofilm as a differential thermocouple to characterize the temperature drops at the two contacts between the nanofilm and the two membranes. This method allows us to address a challenging task of thermal measurement of nanofilms as well as nanowires, and presents a new approach to measuring the contact thermal resistance. Additionally, the microdevice presented here allows for TEM characterization of the nanofilm. This capability enables one to correlate the measured thermoelectric properties with the structural characteristics of the film.

ACKNOWLEDGMENTS

The authors acknowledge funding supports from Office of Naval Research Contract No. 0014-04-1-0532 (Program Manager: Dr. Mihal Gross) and National Science Foundation Award No. CBET 0239179. One of the authors (MTP) is supported by a NSF Graduate Research Fellowship. The authors thank Professor L. Rabenberg for analysis of the TEM images, J. Hurst and Professor A. Holmes for help on Hall measurements, and S. Yu and Professor Y. H. Zhang for growing single-crystal InAs films on lattice-matched GaSb substrates for future studies.

[1] R. Venkatasubramanian, E. Siivola, T. Colpitts, and B. O'Quinn, Nature (London) **413**, 597 (2001); T. C. Harman, P. J. Taylor, M. P. Walsh, and B. E. LaForge, Science **297**, 2229 (2002).
[2] K. F. Hsu *et al.*, Science **303**, 818 (2004); W. Kim, J. Zide, A. Gossard, D. Klenov, S. Stemmer, A. Shakouri, and A. Majumdar, Phys. Rev. Lett. **96**, 045901 (2006); R. G. Yang and G. Chen, Phys. Rev. B **69**, 195316 (2004).
[3] L. D. Hicks and M. S. Dresselhaus, Phys. Rev. B **47**, 12727 (1993); L. S. Hicks, T. C. Harman, X. Sun, and M. S. Dresselhaus, *ibid.* **53**, 10493 (1996).
[4] D. G. Cahill, Rev. Sci. Instrum. **61**, 802 (1990).
[5] D. G. Cahill, Rev. Sci. Instrum. **75**, 5119 (2004).
[6] Y. S. Ju, K. Kurabayashi, and K. E. Goodson, Thin Solid Films **339**, 160 (1999); Y. S. Ju and K. E. Goodson, Appl. Phys. Lett. **74**, 3005 (1999).
[7] W. J. Liu and M. Asheghi, J. Heat Transfer Trans. ASME **128**, 75 (2006).
[8] L. Shi, D. Y. Li, C. H. Yu, W. Y. Jang, D. Kim, Z. Yao, P. Kim, and A. Majumdar, J. Heat Transfer Trans. ASME **125**, 881 (2003).
[9] L. Shi, C. H. Yu, and J. H. Zhou, J. Phys. Chem. B **109**, 22102 (2005).
[10] J. H. Zhou, C. G. Jin, J. H. Seol, X. G. Li, and L. Shi, Appl. Phys. Lett. **87**, 133109 (2005).
[11] C. H. Yu, S. Saha, J. H. Zhou, L. Shi, A. M. Cassell, B. A. Cruden, Q. Ngo, and J. Li, J. Heat Transfer Trans. ASME **128**, 234 (2006).
[12] F. P. Incropera and D. B. Dewitt, *Introduction to Heat Transfer*, 5th ed. (Wiley, Hoboken, NJ, 2006).
[13] D. G. Cahill, M. Katiyar, and J. R. Abelson, Phys. Rev. B **50**, 6077 (1994).

Downloaded 16 Mar 2007 to 146.6.84.239. Redistribution subject to AIP license or copyright, see http://rsi.aip.org/rsi/copyright.jsp